ORIGINAL ARTICLE

Selected mitochondrial DNA landscapes activate the SIRT3 axis of the UPR^{mt} to promote metastasis

TC Kenny[1], P Hart[2], M Ragazzi[3], M Sersinghe[4], J Chipuk[4], MAK Sagar[5], KW Eliceiri[5], T LaFramboise[6], S Grandhi[6], J Santos[7], AK Riar[1], L Papa[1], M D'Aurello[8], G Manfredi[8], MG Bonini[2] and D Germain[1]

By causing mitochondrial DNA (mtDNA) mutations and oxidation of mitochondrial proteins, reactive oxygen species (ROS) leads to perturbations in mitochondrial proteostasis. Several studies have linked mtDNA mutations to metastasis of cancer cells but the nature of the mtDNA species involved remains unclear. Our data suggests that no common mtDNA mutation identifies metastatic cells; rather the metastatic potential of several ROS-generating mutations is largely determined by their mtDNA genomic landscapes, which can act either as an enhancer or repressor of metastasis. However, mtDNA landscapes of all metastatic cells are characterized by activation of the SIRT/FOXO/SOD2 axis of the mitochondrial unfolded protein response (UPR^{mt}). The UPR^{mt} promotes a complex transcription program ultimately increasing mitochondrial integrity and fitness in response to oxidative proteotoxic stress. Using SOD2 as a surrogate marker of the UPR^{mt}, we found that in primary breast cancers, SOD2 is significantly increased in metastatic lesions. We propose that the ability of selected mtDNA species to activate the UPR^{mt} is a process that is exploited by cancer cells to maintain mitochondrial fitness and facilitate metastasis.

INTRODUCTION

Cancer is lethal due to the ability of cancer cells to enter the circulation and recur as metastatic disease. Recent reports have suggested that changes in mitochondrial biology are associated with this process. A study by Draetta and colleagues[1] in pancreatic cancer indicated that oxidative phosphorylation, autophagy and mitochondrial biogenesis are upregulated in recurrent pancreatic tumors. Likewise, Depinho and colleagues[2] found that tumors, which recurred after surviving the telomere-shortening crisis by activating the alternative lengthening of telomeres pathway, are characterized by an upregulation of mitochondrial biogenesis, oxidative phosphorylation and anti-oxidant machinery. Interestingly, these tumors were also found to upregulate SOD2 and to be drastically sensitive to SOD2 inhibition, suggesting that SOD2 is essential for their survival. In addition, analysis of circulating cancer cells showed a specific upregulation of mitochondrial biogenesis and oxidative phosphorylation through PGC-1α.[3] Notably, this study also found a strong positive correlation between PGC-1α expression and distant metastasis.[3] Therefore, although the switch from oxidative phosphorylation to glycolysis characterizes primary tumors, recent data suggest that disseminated cells, circulating cancer cells and metastatic cells are characterized by elevated oxidative phosphorylation and appear to be highly dependent on the anti-oxidant enzyme, Mn-superoxide dismutase (SOD2). The discovery of oxidative tumors has led to the concept of metabolic flexibility,[4] where tumors able to use both glycolysis and oxidative phosphorylation may represent a more aggressive sub-population due to their ability

to adapt to stress. The mechanism coordinating these changes remains unknown.

Another important link between mitochondrial biology and metastasis has arisen from the observation that introduction of mitochondrial DNA (mtDNA) from a metastatic cell line into a non-metastatic cell line using cybrid technology, was sufficient to confer metastatic capacity to the non-metastatic cells.[5] Following this initial report, several others have described similar findings.[6–12] Further, the nuclear gene expression profiles of cybrids, sharing the same nuclear genome but having different mitochondrial genomes, were found to differ suggesting that mitochondrial stress affects nuclear gene expression.[13] Mutations in mtDNA can lead to a defect in oxidative phosphorylation and accumulation of reactive oxygen species (ROS), which can in turn lead to the oxidation of proteins and their misfolding. Cancer cells, therefore, are predicted to rely on the mitochondrial unfolded protein response (UPR^{mt}) to survive such stress.

The original identification of the UPR^{mt} was made in mammalian cells using the overexpression of misfolded OTCΔ in the mitochondrial matrix.[14,15] These studies led to the identification of CCAAT-enhancer-binding protein homologous protein (CHOP) as the transcription factor responsible for the activation of the chaperone hsp60 and proteases such as a ClpP in response to mitochondrial proteotoxic stress.[14,15] Subsequently, the promoter of hsp60 was used extensively as a marker of the UPR^{mt} in *Caenorhabditis elegans*.[16–24] However, the impressive expansion of the study of the UPR^{mt} using mainly *C. elegans* and has also lead to the misconception that the UPR^{mt} does not exist in mammals. Further, it is now clear that the UPR^{mt}

[1]Division of Hematology/Oncology, Department of Medicine, Tisch Cancer Institute, Icahn School of Medicine at Mount Sinai, New York, NY, USA; [2]Department of Medicine, University of Illinois at Chicago, Chicago, IL, USA; [3]Pathology Unit, Arcispedale Santa Maria Nuova - IRCCS, Reggio Emilia, Italy; [4]Department of Oncological Sciences, Icahn School of Medicine at Mount Sinai, New York, NY, USA; [5]Department of Biomedical Engineering, Laboratory for Optical and Computational Instrumentation, University of Wisconsin, Madison, WI, USA; [6]Department of Genetics, School of Medicine, Case Western Reserve University, Cleveland, OH, USA; [7]National Institute of Environmental Health Sciences, Durham, NC, USA and [8]Brain and Mind Research Institute, Weill Cornell Medicine, New York, NY, USA. Correspondence: Dr D Germain, Division of Hematology/Oncology, Department of Medicine, Tisch Cancer Institute, Icahn School of Medicine at Mount Sinai One Gustave L. Levy Place Box 1079, New York, NY 10029, USA.
E-mail: doris.germain@mssm.edu
Received 19 September 2016; revised 13 January 2017; accepted 20 January 2017; published online 3 April 2017
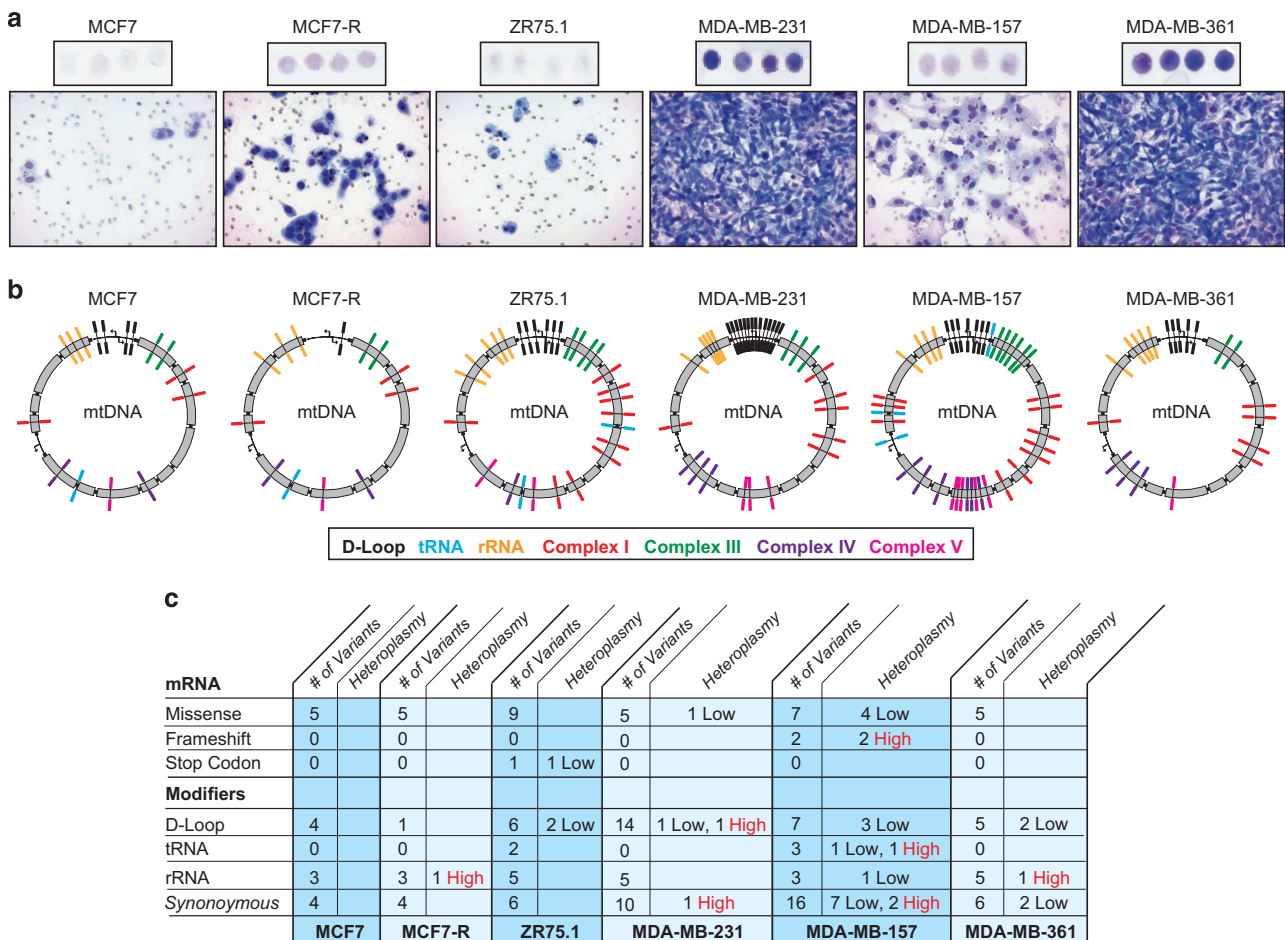
activates much more than proteases and chaperones, and is a complex transcriptional program,[25] which places this pathway as a prime candidate to explain the changes in nuclear gene expression profile of cybrids. In mammalian cells, we and others have used the expression of misfolded proteins in the mitochondria to identify factors of the UPRmt.[14,15,26,27] Namely, we reported a SIRT3/FOXO3a/SOD2 axis of the UPRmt, which is activated independently of the CHOP/hsp60 axis.[27] Considering the regulation of PCG1α by SIRT3,[28–30] the SIRT3 axis of the UPRmt appears favorably placed to explain the upregulation of mitochondrial biogenesis and increased mitochondrial anti-oxidant machinery seen in aggressive disease. Interestingly, a SIRT1/FOXO axis of the UPRmt leading to the activation of SOD2 has also been reported in *C. elegans*.[31] As FOXO transcription factors are regulated by both SIRT3 and SIRT1,[32,33] these observations suggest that this axis of the UPRmt is conserved and may have an important role in both aging and cancer. We therefore initiated the current study to investigate whether the SIRT3 axis of the UPRmt may be associated with specific ROS-generating mtDNA mutations and metastasis. We found that the context in which a mutation is found influences its effect on invasion. As the term landscape is now widely used when referring to variations in the nuclear genome, we propose to use the same concept but in relation to the mitochondrial genome. Therefore, our results suggest that specific combinatorial genomic landscapes of mtDNA, rather than individual missense mutations, are able to activate the SIRT3 axis of the UPRmt and facilitate metastasis. In the context of mitochondrial diseases, it was recently shown that the UPRmt inadvertently maintains deleterious mtDNA species.[19] In the context of cancer, instead, we propose that the UPRmt is exploited to maintain deleterious mtDNA mutations that allow them to advantageously adapt during the metastatic process.

RESULTS

Metastasis of breast cancer cells correlates with mtDNA heteroplasmy

Invasion capacity of cancer cells has been associated with specific mtDNA mutations.[6–12] To determine whether common mutations can be found in multiple invasive breast cancer cells but not in non-invasive cells, we first selected a panel of six breast cancer cells lines and tested their invasion capacity. We found that three cell lines (MCF-7, MCF7R and ZR-75.1) show significantly less invasion than the other three cell lines (MDA-MB361, MDA-MB-231 and MDA-MB-157; Figure 1a). However, MCF-7R cells, which are a clone selected for resistance to endocrine therapy,[34] were more invasive than their parental cell line MCF-7 (Figure 1a). We then performed mtDNA sequencing on all cell lines and compared their

	MCF7		MCF7-R		ZR75.1		MDA-MB-231		MDA-MB-157		MDA-MB-361	
mRNA	# of Variants	Heteroplasmy	# of Variants	Heteroplasmy	# of Variants	Heteroplasmy	# of Variants	Heteroplasmy	# of Variants	Heteroplasmy	# of Variants	Heteroplasmy
Missense	5		5		9		5	1 Low	7	4 Low	5	
Frameshift	0		0		0		0		2	2 High	0	
Stop Codon	0		0		1	1 Low	0		0		0	
Modifiers												
D-Loop	4	1	6	2 Low	14	1 Low, 1 High	7	3 Low	5	2 Low		
tRNA	0		0		2		0		3	1 Low, 1 High	0	
rRNA	3	3	5	1 High	5		3		3	1 Low	5	1 High
Synonymous	4	4	6		10	1 High	16	7 Low, 2 High	6	2 Low		

Figure 1. Invasion capacity correlates with mtDNA heteroplasmy. (**a**) Invasion assays were performed on the indicated cell lines and filters collected at 24 h. Top panel show the overall intensity of 4 independent filters, whereas bottom panels show a magnification of a representative area of one filter. (**b**) Schematic representation of the mtDNA map of the indicated cell lines. Variants and mutations at specific locations along mtDNA are indicated by a line across the map and are color coded according to the area/ gene affected. (**c**) Summary table of number of variants and the level of heteroplasmy in either area encoding mRNA or modifiers. High levels of heteroplasmy are indicated in red. Details of each variant are found in Supplementary Figures 1–4.

sequence with the revised Cambridge reference sequence[35] as the cell lines are derived from different patients and no other internal controls are available. Variants with no known functional consequences that were found in all cell lines were interpreted as background variation related to the difference in the tissue of origin. All remaining variants were classified in three groups as follows: (1) mutations affecting mRNA sequence; (2) modifier variants affecting the sequence in the D-loop, rRNA or tRNA; and (3) synonymous variants representing sequence polymorphisms. Interestingly, the mutations in the ND6 gene (G13997A and 13885insC) previously linked to metastasis were not present in any of the invasive cell lines.[5] In contrast, missense mutations in ATP8 (A8860G) and CYB (A15380G) were present in all cell lines and were homoplasmic (Figures 1b and c, and Supplementary Figures 1–4). However, as these mutations did not distinguish the invasive from the non-invasive cell lines, they alone cannot explain the role of mtDNA mutations in metastasis. Instead, a common characteristic of invasive cells compared with non-invasive cells, including the MCF7R cells, was the presence of at least one variant with significant levels of heteroplasmy (Figures 1b and c, and Supplementary Figures1–4). These observations raise the possibility that the ability of missense mutations in major subunits of the electron transport chain to promote invasiveness may be context dependent and defined by their overall mitochondrial genomic landscapes. In this setting, heteroplasmy may offer the option for the selection of the optimal pro-metastatic mtDNA genomic landscape. Further, the number of lesions per kilobase of mtDNA was higher in invasive cells compared with non-invasive cells (Supplementary Figure 5), which is in agreement with the recent report that low mtDNA repair facilitates invasion.[36]
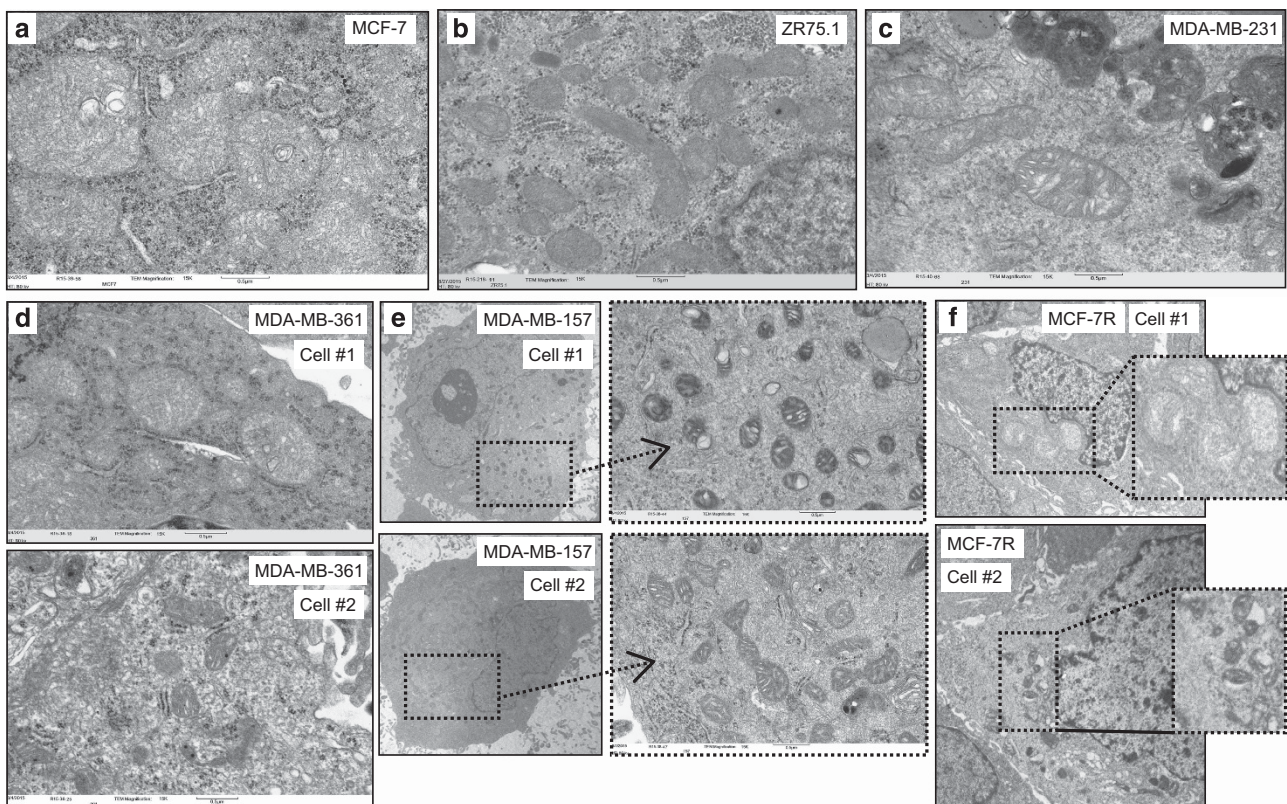
mtDNA heteroplasmy correlates with heterogeneity in mitochondrial morphology in cancer cells

In theory, the presence of homoplasmic mutations in the context of other heteroplasmic variants allows for the combinatorial diversity of mtDNA and the generation of a pool of different mtDNA species within a given cell. If this were the case, we reasoned that such mtDNA diversity could be reflected in a heterogeneous mitochondrial population. To test this possibility, we performed transmission electron microscopy on all cell lines. We found a remarkable heterogeneity in the morphology of the mitochondrial networks among cell lines. The morphology of the mitochondria in MCF-7 cells showed the largest organelles of all cell lines with homogeneous morphology (Figure 2a). The ZR-75.1 cells showed smaller organelles compared with the MCF-7 cells, which were also of homogeneous morphology (Figure 2b). In contrast, all invasive cells showed intra-cellular (MDA-MB-231, Figure 2c) or inter-cellular (MDA-MB-361, MDA-MB 157 and MCF7R; Figures 2d–f) differences in mitochondrial morphology.

This analysis, therefore, is consistent with the hypothesis that heteroplasmy not only generates diverse mtDNA species but may contribute to heterogeneous mitochondrial morphologies.

Mitochondrial heterogeneity correlates with metabolic flexibility and the activation of the UPR^mt

To further investigate the heterogeneity of the mitochondrial population, we next determined the level of oxidative phosphorylation (oxygen consumption rate, OCR) and glycolysis (extracellular acidification rate, ECAR) using the Seahorse XF Analyzer. In three separate experiments including eight replicates in each experiment, we found that the OCR/ECAR ratio was consistent in MCF-7, MCF7R and ZR75.1 cells, and was > 1, indicating a

Figure 2. Mitochondrial morphology varies widely among cell lines and correlates with heterogeneity in invasive cell lines. Electron microscopy at a magnification of 15 K in MCF-7 cells (**a**), ZR-75.1 (**b**), MDA-MB231 (**c**), MDA-MD-361 (**d**), MDA-MB-157 (**e**) and MCF-fulvestrant at magnification of 7K (**f**). In **d**–**f**, images from two independent cells from the same field are shown.
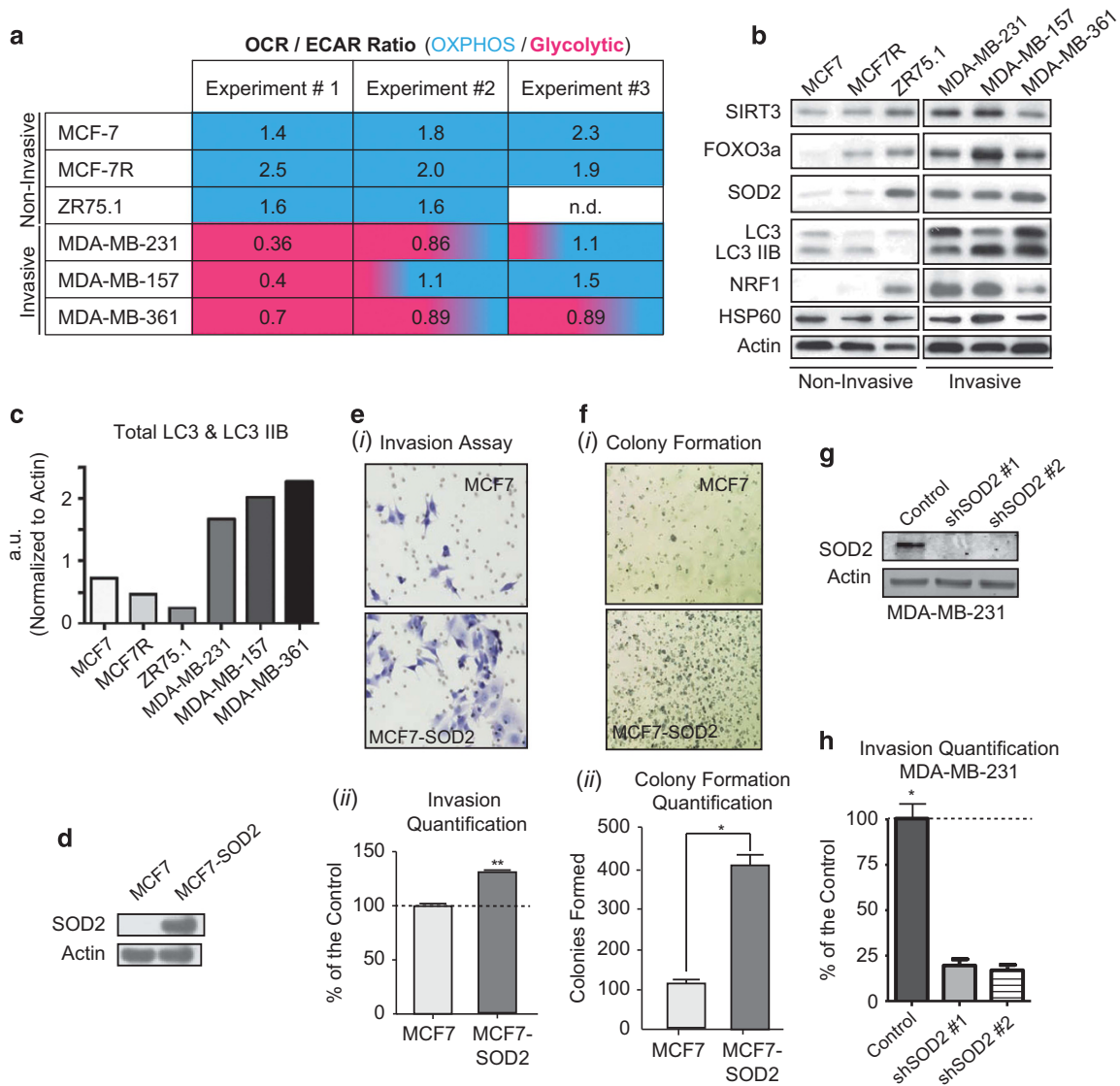
Figure 3. Metabolic flexibility, activation of the SIRT3 axis of the UPR[mt] characterizes invasive cell lines and modulation of SOD2 levels alone alters the invasion capacity. (**a**) OCR/ECAR ratio obtained by Seahorse analysis of the indicated cell lines in three separate experiments; blue indicates a higher use of oxidative phosphorylation over glycolysis and pink indicates a higher use of glycolysis over oxidative phosphorylation; gradient indicates equal use of both. (**b**) Western blot analysis of markers of the UPR[mt] in the indicated breast cancer cell lines. (**c**) Quantification of LC3 and LC3IIB in non-invasive and invasive cell lines. (**d**) Western blotting of SOD2 levels in a stable clone overexpressing SOD2. (**e**) (i) Invasion assay at 24 h in MCF-7 and MCF7-SOD2 cells, (ii) a quantification of the invasion. (**f**) (i) Colony formation assay in MCF-7 and MCF-7-SOD2 cells, and (ii) quantification of colonies. (**g**) Western blotting of SOD2 in MDA-MB-231 cells where SOD2 was inhibited by two independent shRNA. (**h**) A quantification of the invasion with and without shRNA against SOD2 is shown. $*P < 0.05$ calculated by analysis of variance and $**P < 0.01$.

preferential use of oxidative phosphorylation over glycolysis, in these cells (Figure 3a). In contrast, the OCR/ECAR ratio varied widely from one experiment to the other in invasive cell lines, despite identical experimental conditions. One interpretation of this finding is that at any given time, the percentage of cells within the population showing preferential use of oxidative phosphorylation or glycolysis may vary (Figure 3a).

Recently, the presence of deleterious mtDNA mutations has been reported to activate the mitochondrial UPR (UPR[mt]) via the transcription factor ATFS-1 using the hsp60 promoter reporter in C. elegans.[19] The functional homolog of ATFS1 was identified as ATF5 in mammals[17] and acts downstream of CHOP, the original transcription factor identified in mammals for the regulation of hsp60 and matrix proteases.[14,15] In addition to the CHOP axis of the UPR[mt], a SIRT/FOXO/SOD2 axis of the UPR[mt] has been reported

and is conserved between C. elegans and mammals.[27,31] In contrast to the CHOP axis, which regulates chaperones and proteases,[14,15] the SIRT3 axis regulates anti-oxidant machinery (SOD2) via FOXO3a, mitophagy (LC3IIB) and mitochondrial biogenesis via NRF1.[27] Further, SOD2 has been shown to be functionally linked to the activation of glycolysis.[37] We therefore screened the panel of cell lines for markers of the UPR[mt]. No differences in hsp60 were observed between cell lines, suggesting that the CHOP axis of the UPR[mt] does not mediate the differences observed. As hsp60 is the best-characterized marker of the UPR[mt], this result was surprising. We reasoned that as hsp60 is upregulated early in cancer progression in human cancer,[38,39] and that our analysis was performed in established cancer cell lines, hsp60 may also be activated early during transformation in cell lines. To test this possibility, we analyzed the level of hsp60

following induction of the oncogene ras in the non-transformed cell line MCF10A. We found that hsp60 is indeed upregulated within hours (Supplementary Figure 6a). However, we found that MDA-MB-231, MDA-MB-157 and MDA-MB-361 cells were positive for all five markers of the SIRT/FOXO/SOD2 axis of the UPR^{mt} (Figure 3b). However, this was not simply due to differences in mitochondrial mass since other mitochondrial markers such ATP5O, COX1 and cytochrome *c* did not distinguished the invasive from the non-invasive cell lines (Supplementary Figure 6b). Interestingly MCF7R cells show an increase in the level of four of these markers relative to the MCF-7 parental cell line (Figure 3b). The non-invasive ZR75.1 cells, however, showed four out of the five UPR^{mt} markers to be elevated but failed to activate autophagy. Given that these cells carry several missense mutations and one stop codon mutation (Supplementary Figure 2), this result suggests that their inability to eliminate irreversibly damaged mitochondria from the network by autophagy may limit their ability to survive invasion. In support of this possibility, the MDA-MB157 cells also carry several missense mutations and one stop codon mutation (Supplementary Figure 3) but show elevated levels of autophagy and are invasive. Overall, the quantification of autophagy was higher in the invasive cell lines (Figure 3c).

As SOD2 has been shown to promote metabolic flexibility,[37] we next tested whether SOD2 alone is able to increase invasion and created MCF-7 stable clones expressing SOD2 (Figure 3d). We found that expression of SOD2 did in fact increase the invasion capacity of these cells (Figure 3ei, ii), as well as their ability to form colonies on soft agar (Figure 3fi, ii). Further, inhibition of SOD2 by shRNA in MDA-MB-231 cells significantly decreased their invasion capacity (Figures 3g and h). Despite increasing relative invasion, SOD2 overexpression alone in the MCF-7 cells was not sufficient to increase the invasion to the same level as in the metastatic cell lines such as MDA-MB-231. Our interpretation of these results is that SOD2 is important, but the other downstream effectors of the UPR$^{mt-SIRT3}$ are also required.

Metastatic potential of ROS-generating mtDNA mutation is context dependent

Our data suggest that the metastatic potential of missense mutations in major subunits of the electron transport chain is dependent on its surrounding mtDNA landscape and the activation of the SIRT3 axis of the UPR^{mt}. However, as the nuclear genomic landscape of the cell lines in our panel is also widely different, a significant contribution of the nuclear genome to the activation of the UPR^{mt} remains a distinct possibility.

Therefore, to further interrogate the role of the mtDNA landscape on the activation of the UPR^{mt}, we took advantage of a collection of cybrids derived from the 143B/206 osteosarcoma cells lacking mtDNA.[40] Given that we found a missense mutation in cytochrome *B* (CyB) present in all breast cancer cell lines in our panel, we first focused on one cybrid line where the mtDNA was repopulated with mtDNA from a patient carrying a frame-shift mutation in CyB and is therefore referred to as CyB.[40] As in the breast cancer cell lines, the CyB line is homoplasmic for this mutation. In addition to this cybrid, a hybrid called Hybrid B, between the CyB line and another cybrid was generated, leading to a variant of the CyB carrying a mixed mtDNA landscape.[40] A schematic representation of the various lines is shown in Figure 4a. First, the expression of the markers of the UPR^{mt} was analyzed by western blotting. We found that both the cybrid CyB and the Hybrid B show elevated expression of all markers of the SIRT/FOXO/SOD2 axis of the UPR^{mt} compared with the parental cell line (wild type (WT)), with the exception of SOD2, which was not significantly elevated in Hybrid B cells compared with the WT cell line (Figures 4b and c). Further, hsp60, ATP5O, COX1 and cytochrome *c* were not significantly different between invasive

and non-invasive cell lines (Figures 4b and c, and Supplementary Figure 6c). We next determined the invasion capacity of each cell line. Remarkably, we found that both CyB and Hybrid B were significantly more invasive compared with the parental cell line at both 24 and 48 h (Figures 4d and e). However, the invasiveness of Hybrid B was lower than CyB most noticeably at 24 h supporting our observation that levels of SOD2 impact invasion in MCF7 cells (Figure 3e). However, as Hybrid B remains much more invasive than WT cells, whereas SOD2 does seem to have an important role, it is clearly not the only factor and the additional factors of the UPR^{mt} impact invasion.

We then sequenced the mtDNA in CyB, Hybrid B and the WT parental cell line. We found that CyB and Hybrid B were remarkably similar with only a few differences in heteroplasmy (Figures 4f and g, and Supplementary Figures 7 and 8). Given that both lines carry the same missense mutation in CyB and share the same nuclear DNA, this result indicates that the effect of a ROS-generating mutation on invasion is context-dependent and the presence of even small differences in the mtDNA landscape affects the extent of the activation of the SIRT3 axis of the UPR^{mt} and invasion.

To expand our analysis, we also performed the same analysis on a separate cybrid of the same recipient 143B/206 osteosarcoma cells lacking mtDNA that was repopulated with mtDNA from a patient harboring a stop codon in COX1 and is therefore referred as COX1 line.[40] The COX1 cybrid was also used to construct another hybrid called Hybrid E (Figure 5a). Interestingly, in this pair we found a similar trend in the elevation of the UPR^{mt} markers (Figures 5b and d) and did not show difference in other mitochondrial markers (Supplementary Figure 6d). In contrast to the CyB and Hybrid B cells, the overall difference in the levels of FOXO3a was not as pronounced; however, the molecular weight of FOXO3a was slightly lower in COX1 and HybrideE, which is consistent with the deacetylation of FOXO3a. Importantly, deacetylation of FOXO3a is required for its nuclear localization and transcription of SOD2. To test this possibility, the presence of acetylated FOXO3a was tested and we found that in both COX 1 and Hybrid E, the levels of acetylated FOXO3a are decreased (Figures 5c and d). Further, although both cell lines were more invasive than the parental cell line, (Figures 5e and f), Hybrid E was also less invasive than COX1 cells at 24 h (Figure 5e). Sequencing of both cells and the WT parental clone showed that these cells are remarkably similar with only a few minor differences in the heteroplasmy of variants (Figures 5g and h, and Supplementary Figures 7 and 9). Therefore, as was seen in the CyB mutation, the invasive effect of the COX1 mutation is sensitive to its mtDNA landscape and correlates with the extent of the activation of the UPR^{mt}.

Elevated expression of SOD2 is associated with oncocytic tumors with poor prognosis, NAD+ staining and metastasis

Having established that activation of the SIRT3/FOXO3a/SOD2 axis of the UPR^{mt} is associated with invasion, we aimed at validating this axis in primary breast cancers. We reasoned that, if the UPR^{mt} promotes mitochondrial biogenesis, tumors showing increased mitochondrial mass, such as oncocytic tumors, might be characterized by the activation of the UPR^{mt}. Oncocytic tumors of the thyroid and other endocrine tissues are usually benign. However, in the breast, oncocytic tumors and mitochondria-rich tumors were found to have a worse prognosis.[41] This observation suggests that the amount of mitochondria alone is not sufficient to predict outcome but rather the quality and fitness of the mitochondrial network may be most relevant. If so, we hypothesize that oncocytic breast cancers may not only upregulate mitochondrial biogenesis but also oxidative phosphorylation and the anti-oxidant machinery simultaneously through activation of the UPR^{mt}. To test this possibility, we used a unique collection
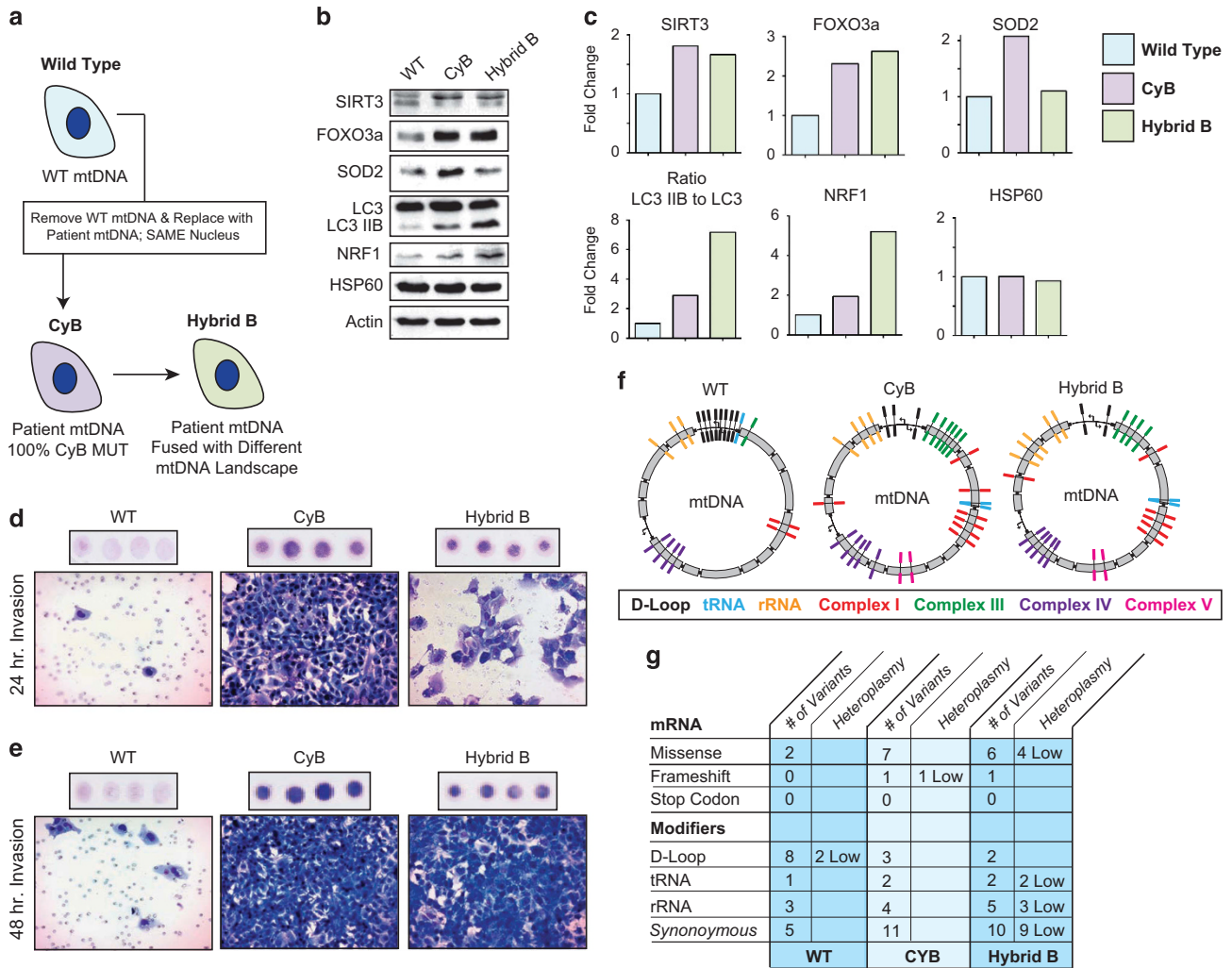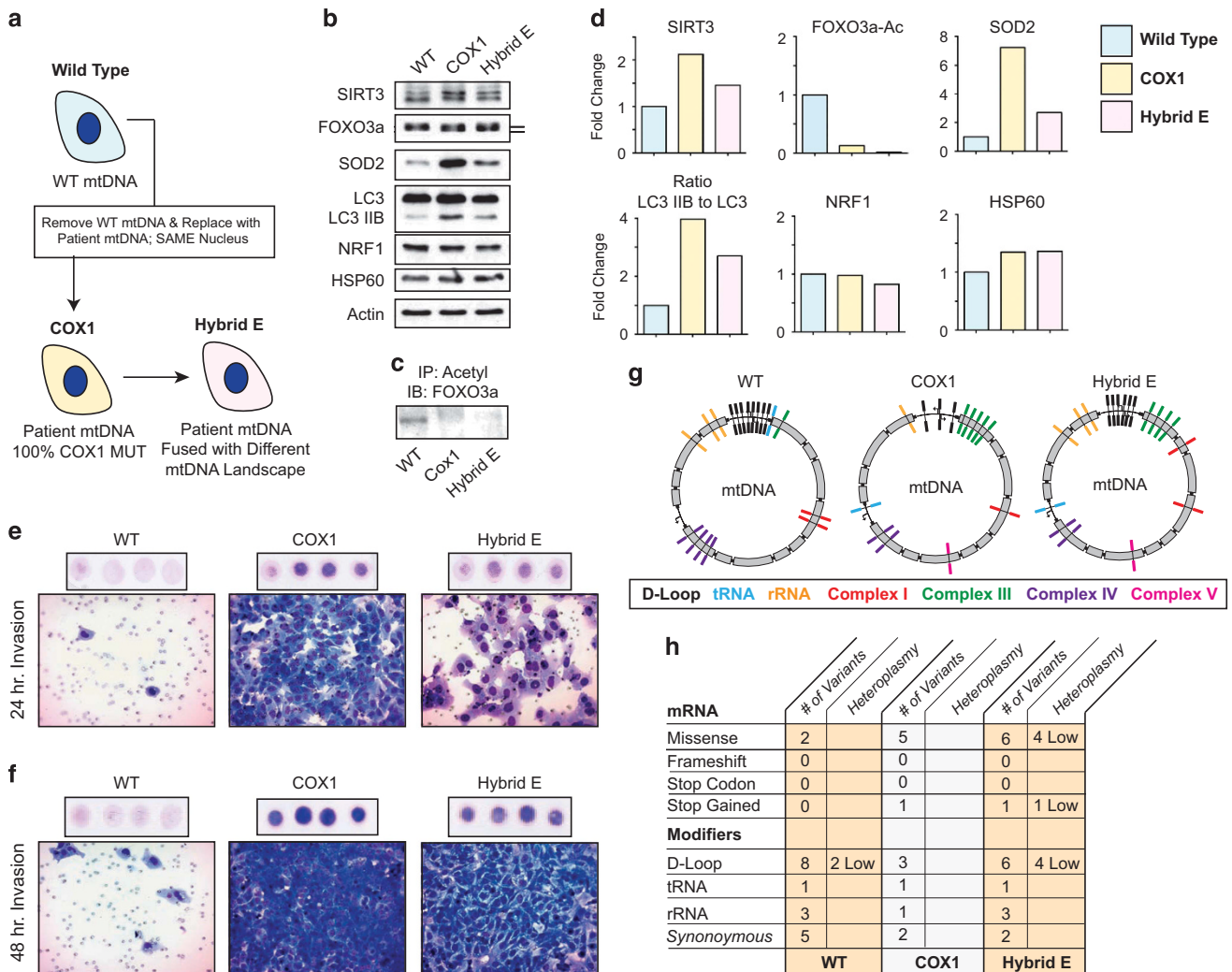
Figure 4. Increased invasion capacity and activation of the UPR^mt of cybrids. (**a**) Schematic representation of the generation of the CyB cybrid and their fusion resulting in hybrid B. (**b**) Western blotting of the markers of the UPR^mt in the indicated cell lines. (**c**) Quantification of the levels of the UPR^mt shown in **b**. (**d**) Invasion assays of the indicated cell lines after 24 h. Top panel represents an overall view of four independent filters. Bottom panel represent a magnification of a representative area of a single filter. (**e**) Invasion assays of the indicated cell lines after 48 h. Top panel represents an overall view of four independent filters. Bottom panel represent a magnification of a representative area of a single filter. (**f**) Schematic representation of the mtDNA map of the indicated cell lines. Variants and mutations at specific locations along mtDNA are indicated by a line across the map and are color code according to the area/ gene affected. (**g**) Summary table of number of variants and the level of heteroplasmy in either area encoding mRNA or modifiers. Details of each variant are found in Supplementary Figures 7 and 8.

of oncocytic, mito-rich and mito-poor breast cancers, and performed SOD2 staining as a marker of the SIRT3 axis of the UPR^mt. We found a statistically significant increase in SOD2 staining in the oncocytic tumors compared to the mito-rich and mito-poor samples (Figures 6a and b). This observation was not simply due to the increase in mitochondrial mass in this sub-population, because SOD2 staining in normal ducts, which show low number of mitochondria, also had elevated SOD2 staining (Figures 6a and b). This analysis also revealed the presence of strongly positive SOD2 foci within tumors that are otherwise negative for SOD2 (Figure 6a). This pattern raised the possibility that SOD2 may identify heterogeneity within the cancer cell population of a primary tumor. Further, as SOD2 staining was found to be upregulated in recurrent cancers,[2] the expression of SOD2 may allow for the survival of cells through the metastatic process. Therefore, we aimed at evaluating whether SOD2 positivity predicts overall survival. SOD2 staining was scored for extent (percentage of positive cells) and intensity (1+, 2+ or 3+), and patients were classified in two groups. The first group was classified as high SOD2 expressers (SOD2^high) based on the presence of any extent of 3+ staining or intensity × extent score of > 100. The second group was classified as low SOD2 expressers (SOD2^Low) based on an intensity × extent score of less than 100. This classification revealed a statistically significant worse outcome of patients with SOD2^High staining (Figure 6c). Importantly, the presence of small foci of intense SOD2 staining within otherwise largely negative tumors is sufficient to predict worse clinical outcome.

SOD2 requires deacetylation by SIRT3[42] in order to be active. Sirtuins require NAD+ for their activity. In their analysis of the SIRT1/FOXO axis of the UPR^mt, Auwerx and colleagues[31] showed that modulating the NAD+/NADH ratio affects longevity by activating the UPR^mt. In cancer biology, elevated NADH level is used as a surrogate marker of glycolysis, whereas NAD+ correlates with an increased oxidative state.[43] Therefore, we further reasoned that areas of the tumors that are positive for SOD2 could also be positive for NAD+ rather than NADH for two reasons. First, NAD+ is required for SIRT3 to deacetylate SOD2 and, second, NAD+

Figure 5. Increased invasion capacity and activation of the UPRmt of cybrids. (a) Schematic representation of the generation of the COX1 cybrid and their fusion resulting in hybrid E. (b) Western blotting of the markers of the UPRmt in the indicated cell lines. (c) Immunoprecipitation of pan-acetylated proteins followed by western of FOXO3a. (d) Quantification of the levels of the UPRmt shown in b and c. (e) Invasion assays of the indicated cell lines after 24 h. Top panel represents an overall view of four independent filters. Bottom panel represent a magnification of a representative area of a single filter. (f) Invasion assays of the indicated cell lines after 48 h. Top panel represents an overall view of four independent filters. Bottom panel represent a magnification of a representative area of a single filter. (g) Schematic representation of the mtDNA map of the indicated cell lines. Variants and mutations at specific locations along mtDNA are indicated by a line across the map and are color code according to the area/ gene affected. (h) Summary table of number of variants and the level of heteroplasmy in either area encoding mRNA or modifiers. Details of each variant are found in Supplementary Figures 7 and 9.

would indicate area of the tumor that activates oxidative phosphorylation. If so, NAD+ may be used as a surrogate marker of the activation of the UPRmt along with SOD2. Fluorescent lifetime imaging microscopy (FLIM) can produce an image based on the differences in the exponential decay rate of the fluorescence from a fluorescent sample including that of endogenous fluorophores such as NADH.[43] The detection of free and bound NADH by FLIM has been used to measure for a number of metabolic profiling experiments including measuring glycolysis in cancer sections. In this study, the oncocytic, mito-rich and mito-poor breast cancers were tested by FLIM. We found an impressive overlapping between areas that are positive for SOD2 by immunohistochemistry (IHC) and NAD+ by FLIM (Figure 6d). These results suggest that the activation of the SIRT/FOXO/SOD2 axis of the UPRmt can be detected in primary breast cancers.

As our hypothesis is that the SOD2High population will survive the metastatic process, we next aimed at testing whether SOD2 staining is indeed enriched in metastatic lesions compared with the primary tumors of the same patient. We tested 50 such matched samples (100 cores) and found a statistically significant increase in SOD2 staining in the metastatic lesions compared with the primary tumors (Figures 6e and f). Further, we found that SOD2 staining of the primary tumors correlated with lymph node status (Figure 6g). This analysis strongly supports our hypothesis of the clonal selection of SOD2High sub-populations, which activate the UPRmt, during metastasis.

DISCUSSION

The first report that transfer of mtDNA from metastatic cell line to a non-metastatic cell line was able to modify invasion capacity linked this effect to a specific ROS-generating mtDNA mutation in the ND6 gene (G13997A and 13885insC).[5] Since then, several other groups have reported similar findings although using different mtDNA mutations.[6–12] Of interest, one group reported that mild mtDNA mutations were actually more potent at generating
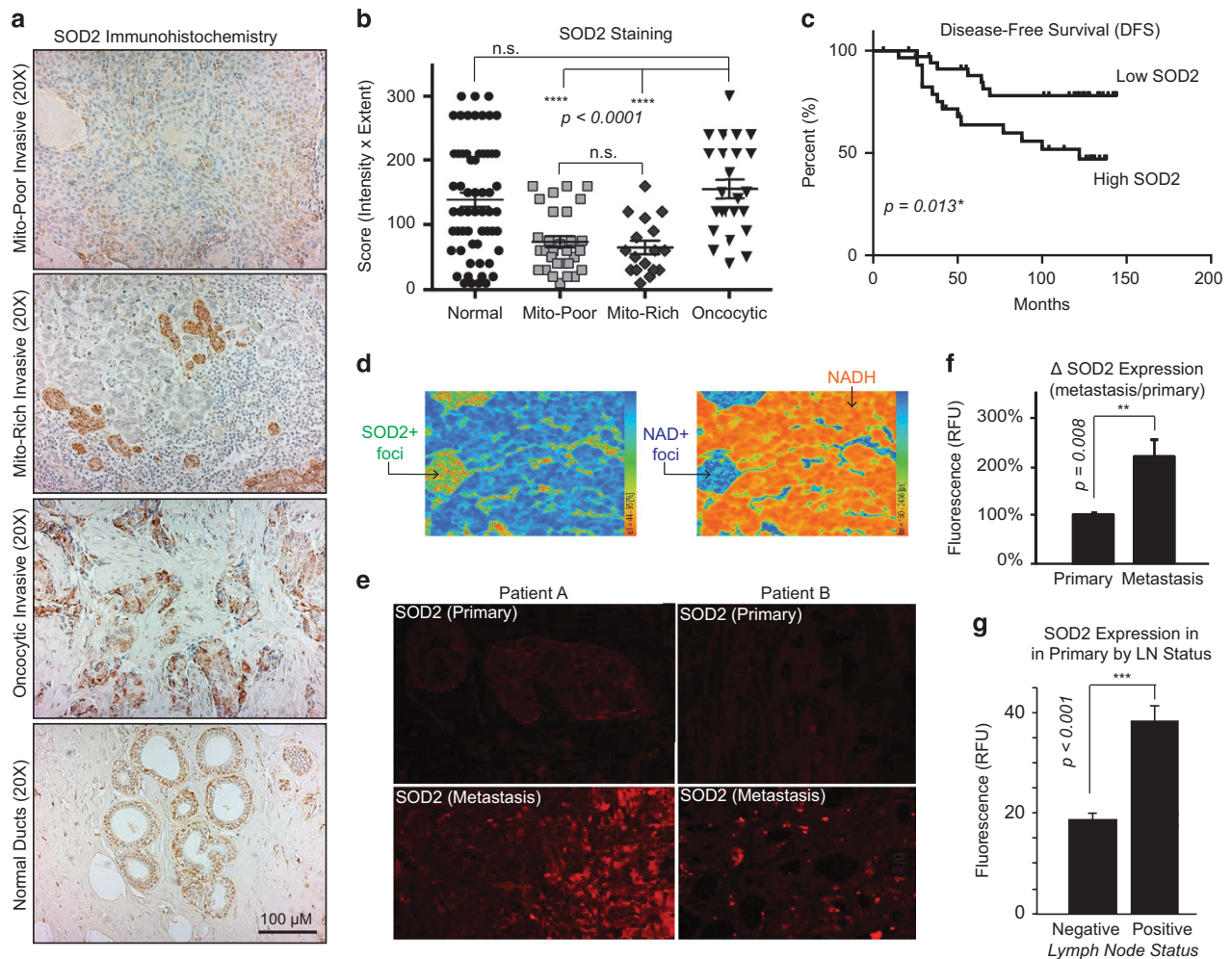
Figure 6. SOD2 staining is associated with worse prognosis and is enriched specifically in metastases. (**a**) IHC of SOD2 in mito-poor, mito-rich, oncocytic breast cancers and in normal ducts. (**b**) Quantification of SOD2 staining of individual patients and adjacent normal ducts. (**c**) Disease free survival rate of patients with high SOD2 (any extent of 3+ staining of SOD2 or a intensity x extent score of more than 100) versus SOD 2 (intensity × extent score of < 100). (**d**) FLIM analysis of mito-rich tumors show overlapping between SOD2-positive foci and NAD+ area, whereas the remainder of the tumors is negative for both. (**e**) Immunofluorescence staining of SOD2 in matched primary/metastatic breast tumors from the same patients. (**f**) Quantification of the ratio of SOD2 expression in metastatic/primary tumor tissue ($n = 50$ patients, 100 matches pairs). (**g**) Graph of SOD2 expression in primary tumors according to nodal status.

aggressive tumors compared to cells carrying mutations causing severe defect in OXPHOS.[11] Although in most studies the mechanism remained unclear, some have suggested that mtDNA mutations affecting OXPHOS act on invasion via a cross-talk between cancer cell mitochondria and the extracellular matrix.[12] More recently, it was suggested that synonymous mtDNA variants found in different mouse strains also affects the metastatic potential of tumors.[44,45] Although it is now recognized that mtDNA can influence metastasis, the nature of the type of mtDNA mutations involved and the mechanism as to how these effects are exerted remains controversial.

Data presented here offer an alternative model that may reconcile these various observations. Our data show that the ability of strong or mild missense mutations such as those in CyB to promote invasion is highly dependent on its surrounding mtDNA landscape. This conclusion is based on the fact that CyB cells and Hybrid B cells share the same mutation in CyB and the same nuclear genomes but differ in their invasion capacity (most visible at 24 h), which is associated with subtle differences in mtDNA. Our results suggest that some mtDNA landscapes act as enhancers of the missense mutations, whereas others act as repressors. Therefore, our data suggest that rather than being

associated with specific mutations alone, metastasis may require specific mtDNA combinatorial landscapes. The common denominator of these landscapes is their ability to activate the SIRT3/FOXO3A/SOD2 axis of the UPR[mt].

Recently, the mtDNA repair machinery was reported to be reduced during disease progression and forced expression of mtDNA repair enzymes in mice delayed metastasis.[36] Therefore, defects in mtDNA repair, as suggested by the increased steady-state level of mtDNA lesions in the UPR[mt]-positive cell lines (Supplementary Figure 5), may be a critical partner in the generation of heteroplasmy and pro-metastatic mtDNA landscapes. Our data suggest that in this context, heteroplasmy even at very low frequency can have significant effects on the invasion capacity. Interestingly, analysis of both Hybrids E and B initially revealed heteroplasmy at the COX1 and CyB mutations.[40] However, complete sequencing of the mtDNA genomes of these clones was not performed. Our data revealed homoplasmy at the COX1 and CyB mutations, and a remarkable similarity between the COX1 cybrid and hybrid E, and the CyB cybrid and hybrid B, respectively, suggesting mtDNA heteroplasmic drift toward higher mutation levels. This observation raises the possibility that mtDNA drifting and heteroplasmy work hand in hand toward the selection

of the optimal mtDNA landscape favoring metastasis. This is in agreement with a more recent study indicating a wide range of heteroplasmy in breast cancer.[46] Our data are also in line with the observation that mtDNA polymorphisms affect the risk of breast cancer.[47,48]

Based on our results and the observations by others, we propose the following model: homoplasmic mtDNA landscapes unable to activate the SIRT3 axis of the UPR[mt] have little capacity to adapt to mitochondrial stress and as a result do not survive metastasis (Figure 7, sub-population 1). However, homoplasmic mtDNA landscapes able to lead to the activation of the SIRT3 axis of the UPR[mt] have increased mitochondrial fitness and can adapt to stress and survive metastasis (Figure 7, sub-population 2). As mtDNA repair capacity has been linked to metastasis,[36] the prediction is that the number of mtDNA mutations will increase leading to heteroplasmy (Figure 7, sub-population 2). Heteroplasmy may lead to generation of mtDNA landscapes that fail to activate the SIRT3 axis of the UPR[mt] and others that do (Figure 7, sub-population 2). We propose that those that do not are eliminated from the population as the disease progresses, while the others survive. Within the surviving cells, mtDNA drifting may underlie a selection mechanism toward the optimal mtDNA landscape.

Although some studies have suggested that mtDNA may directly lead to the activation of nuclear encoded genes involved in metastasis,[12,49] we propose an additional possibility; by activating the SIRT3 axis of the UPR[mt], the pro-invasive mtDNA landscapes promote increased mitochondrial fitness, which indirectly supports cells through the metastatic process. This possibility will be tested in the future.

We found that the levels of SOD2 appear to be an important, but not the only, determinant of invasion capacity. We previously described that SIRT3 acts upstream of FOXO3a, and that the transcription of SOD2 is dependent on FOXO3a.[27] In some cells however, SOD2 does not correlate with FOXO3A. One potential explanation is that the regulation of sub-cellular localization of FOXO3a by Akt may alter its effect on SOD2. Further the regulation of SOD2 by the UPR[mt] may not be restricted to FOXO3a. These possibilities will be addressed further in the future.

Although others have also implicated the sirtuins, the transcription factors FOXO3a and SOD2 in the UPR[mt], the validation of this pathway in human cancer was lacking.[27,31] The present study supports the notion that the activation of the SIRT3 axis of the UPR[mt] is associated with increased mitochondrial heterogeneity, metabolic flexibility and metastasis.

We found that SOD2 is significantly enriched in metastatic lesions compared with primary tumors, and that areas of SOD2 positivity correlate with NAD+ rather than NADH by FLIM. This finding is in agreement with the observation that affecting the NAD+/NADH balance using NAD+ precursors inhibits metastasis.[9]

The DePinho group reported that elevated SOD2 protein levels are found in recurring tumors but are low in primary tumors in mouse models, and that these recurring lesions are extremely sensitive to inhibition of SOD2.[2] We found that elevated SOD2 correlates with worse prognosis, even if the expression of SOD2 is limited to small foci in the primary tumors and the bulk of the tumor is negative for SOD2. These findings are also consistent with our observation that metastatic tumors have higher SOD2 protein levels in metastatic lesions when compared with the primary tumor of the same patient (Figures 6e and f). Therefore, we hypothesize that SOD2 may be important to support the survival of metastatic and recurrent cancer cells.

This leads to the question of how this model can reconcile with the findings by Haigis and colleagues[50] and our own pervious report that SIRT3 and SOD2 are downregulated in the vast majority of breast cancers.[51] We propose a model whereby, although a decrease in SIRT3 and SOD2 may be required to increase superoxide and facilitate the switch to glycolysis early during disease progression as suggested by Haigis and colleagues,[50] SOD2 expression is re-activated later to allow for metabolic flexibility. In support of this hypothesis, Bonini and colleagues[37] recently reported the ability of SOD2 to promote glycolysis. In this study, modulation of SOD2 levels was shown to allow metabolic flexibility.[37] Further, Haigis and colleagues[52] have also reported recently that SIRT3 is activated upon depolarization of the mitochondria, a result that is consistent with the role of SIRT3 in the UPR[mt]. Therefore, we propose that the mitochondria heterogeneity within the same cell population may provide a
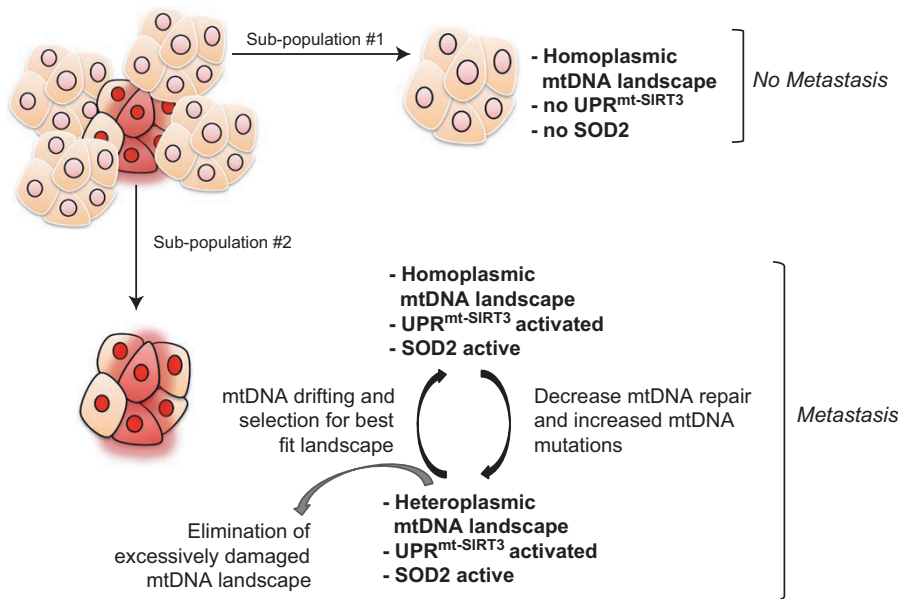
Figure 7. Model of mitochondrial heterogeneity in cancer based on mtDNA status. In this model, sub-population 1 carries homoplasmic mtDNA and do not activate the SIRT3 axis of the UPR[mt] or SOD2. This sub-population is more sensitive to therapy. In sub-population 2, mtDNA is heteroplasmic leading to the generation of different mtDNA species. Some of these combinations lead to the activation of the SIRT3 axis of the UPR[mt] and metabolic flexibility, which facilitates metastasis.

larger 'tool-box' that facilitates adaptation to stress and metabolic flexibility.

Recently, the UPR[mt] has been proposed to maintain deleterious mutations in the context of mitochondrial diseases.[19] Our data suggest that cancer cells may utilize a similar mechanism toward the selection of cells with increased metastatic potential. Importantly, although the UPR[mt] was initially identified as a result of the accumulation of misfolded proteins in the matrix and the activation of chaperone and proteases,[15] we and others have now established that the UPR[mt] activates several genes other than chaperones and proteases.[25–27] An important role of the matrix protease ClpxP in metastasis has been reported recently.[53] Although we did not find changes in hsp60, which is expected to be in the same axis of as ClpxP, it is important to note that in breast cancer cells, the main difference in ClpxP was observed between MCF10A and MCF7 cells.[53] Therefore, it is possible that changes in the hsp60/ClpxP axis of the UPR[mt] are an early event, a possibility supported by our observation that hsp60 is activated a few hours after activation of ras (Supplementary Figure 6). This possibility will be investigated further in the future. Collectively, it is becoming clear that the UPR[mt] is a complex transcriptional program encompassing several parallel axes fulfilling different aspects of this large program.

Collectively, the results presented in the current study indicate that the activation of the SIRT3 axis of the UPR[mt] is linked to metastasis. Therefore, agents able to target the UPR[mt] could represent promising candidates for therapy.

MATERIALS AND METHODS

Reagents, cell culture and western blotting

Breast cancer cell lines were cultured in either Dulbecco's modified Eagle's medium (DMEM; MDA-MB-231, MDA-MB-361, MDA-MB-157, MCF7 and MCF7R) or RPMI medium (ZR75.1) supplemented with 10% fetal bovine serum and 100 units/ml penicillin and 100 μg/ml streptomycin. WT osteosarcoma cell lines and cybrids COX1 and CyB, and Hybrids B and E cultured in DMEM supplemented with 10%, 100 units/ml penicillin, 100 μg/ml streptomycin and 50 μg/ml uridine. Western blot analyses were performed as described previously,[26] using the following antibodies: SIRT3 (Cell Signaling, Danvers, MA, USA), LC3B (MBL International, Woburn, MA, USA), FOXO3A (Cell Signaling), SOD2 (Millipore, Billerica, MA, USA), Hsp60 (BD Transduction Laboratories, San Jose, CA, USA), NRF1 (Abcam, Cambridge, MA, USA), and Actin (Millipore).

Invasion assay

A transwell *in vitro* invasion assay was used to characterize invasion. Growth factor-reduced matrigel basement membrane matrix (BD Biosciences) was diluted 1:100 in cold PBS and 200 μl was added to the top of the cell permeable membrane (0.3 μm pore size) inside cell culture inserts for 24-well plates (Falcon). These inserts were incubated at for 2 h at room temperature, to allow polymerization of the artificial extracellular matrix. Following incubation, excess matrigel solution was removed by pipette. Cells split the day prior were then trypsinized and collected in serum-free DMEM supplemented with 100 units/ml Penicillin/Streptomycin (Gibco, Carlsbad, CA, USA) and then spun at 2000 r.p.m. for 5 min. Media was aspirated and cells were resuspended in DMEM supplemented with only 100 units/ml Penicillin/Streptomycin and counted using a hemocytometer and tryphan blue (Invitrogen). Fifty-thousand cells in 0.5 ml of serum-free DMEM were plated inside cell culture insert atop polymerized matrigel solution. Five-hundred microliters of 10% fetal bovine serum in DMEM supplemented with 100 units/ml Penicillin/Streptomycin was added to the 24-well plate outside cell culture inserts and invasion assay was incubated at 37 °C and 5% CO_2 for 12, 24 or 48 h. (For invasion assays using WT osteosarcoma cells, Cybrids CyB or COX1 and Hybrids B or E culture medium was supplemented with 50 μg/ml uridine).

Histology and IHC staining

Histological slides were obtained from the Department of Anatomic Pathology at Bellaria Hospital, University of Bologna (Italy). For immunostaining of paraffin-embedded sections with SOD2 (Millipore 06-984),

samples were deparaffinized in xylene and rehydrated in water, and antigen retrieval was performed in citrate buffer. Endogenous peroxidase activity was blocked with 3% hydrogen peroxide for 10 min. All washes were performed using 50 mM Tris-HCl, pH 7.6, three times for 2 min. Blocking solution was applied for 30 min before the incubation with SOD2 antibody at a dilution of 1/100 for 2 h at room temperature. Secondary antibody was incubated for 1 h and the sections developed using the LSAB + kit peroxidase (DAKO, Glostrup, Denmark; catalogue number K0690) for 10 min. Sections were then counterstained in hematoxylin and mounted with Permount (Fischer Scientific, Waltham, MA, USA; catalogue number SP15-100).

Scoring of IHC staining

Immunostain for antimitochondrion antibody was scored as previously described.[41] To score SOD2 immunostaining, the intensity and percentage of IHC staining were recorded. The intensity was scored from 0 to 3+ and defined as follows: 0, no staining; 1+, weak staining; 2+, moderate staining; 3+, strong staining based on the granular cytoplasmic staining evaluation. In addition, the quickscore (Q score) based on estimating the percentage (P) of tumor cells showing characteristic staining (0–100%) and by estimating the intensity (I) of staining was adopted for IHC semi-quantification. The slides were scored by multiplying the percentage of positive cells by the intensity ($Q = P \times I$; maximum = 300). Multiplying staining intensity per percentage of stained cells we obtained a score 0–300. SOD2 expression was recorded as high, based on the presence of any extent of 3+ staining or a Q score >100. SOD2 expression was recorded as low, when Q score < 100.

Fluorescent lifetime imaging microscopy

FLIM analysis was performed on slides stained for SOD2 by IHC as to identify the area of interest. All FLIM images were collected in a multiphoton optical workstation at the Laboratory of Optical and Computational Instrumentation at University of Wisconsin–Madison. The excitation source was a Ti:Sapphire laser (Spectra Physics; Maitai) tuned to wavelength of 740 nm. The excitation and emission were coupled through an inverted microscope (Nikon, Shinagawa, Japan; Eclipse TE300) with a ×40 water-immersion objective (Nikon; Apo, Lambda S, numerical aperture 1.25). A 470/50 nm bandpass emission filter (Chroma, Burlington, VT, USA) was also used to selectively collect NADH fluorescence. FLIM images were collected at 256×256 resolution with 150 s collection using SPC-830 Photon Counting Electronics (Becker and Hickl GmbH, Berlin, Germany) and Hamamatsu H7422P-40 GaAsP photomultiplier tube (Hamamatsu Photonics, Bridgewater, NJ, USA). Urea crystals were used to determine the Instrumentation Response Function with a 370/10 bandpass emission filter (Semrock, Rochester. NY, USA).

SPCImage software (Becker & Hickl GmbH) was used to analyze the fluorescence lifetime decay curves. The lifetime decay of each pixel was fit with a double exponential decay, which resulted in a tau-mean of 1.3 with s.d. of 0.2. The two component of the double exponential decay refers to short and long lifetime component (1and 2, respectively). Unnecessary pixels were excluded using thresholding and the nearest 3×3 pixel were used with a binning of 2 for the analysis. An incomplete exponential model was used for the analyzing the FLIM data.

Seahorse analysis

Cells were seeded in 200 μl of complete media (RPMI for ZR75.1, DMEM for all other cell lines) in XF96 plates (Seahorse Bioscience, Santa Clara, CA, USA). Cells were seeded 24 h before assay to obtain ~ 50–60% confluency on day of assay; seeding densities: HBL-100 4.5×10^3, MCF7 4×10^3, MCF7-R 4.5×1^3, ZR75.1 7×10^3, MDA-MB-231 4×10^3, MDA-MB-361 3.5×10^3, MDA-MB-157 3.5×10^3 and MDA-MB-453 3.5×10^3. OCR and ECAR were measured using the XF96 Extracellular Flux Analyzer and the XF Cell Mito Stress Test Kit (Agilent/Seahorse Bioscience, Chicopee, MA, USA) according to manufacturer's instructions with optimized concentrations of metabolic inhibitors: Oligomycin 2 μM, carbonilcyanide p-triflouromethoxyphenylhydrazone (FCCP) 2 μM, Rotenone/Antimycin A 0.5 μM (Seahorse Bioscience). Following the assay, cell density was calculated as previously described.[54] OCR and ECAR measurements were normalized to calculated cell densities. Reported OCR/ECAR ratios represent the ratio between basal OCR rate and basal ECAR (before addition of any metabolic inhibitors). All experiments were performed with cell line-specific measurements done in eight replicates.

mtDNA sequencing and analysis

For each sample, 1 ng of DNA was indexed using the Nextera XT library preparation kit (Illumina, San Diego, CA, USA). During the Nextera procedure, after the tagmentation, amplification and PCR cleanup steps, fragment size distribution was assessed using the Bioanalyzer (Agilent, Santa Clara, CA, USA) and total DNA concentration was determined using the PicoGreen assay. Inputs were normalized accordingly. The remainder of the library preparation was performed as per the manufacturer's protocols. DNA sequencing was performed on the Illumina MiSeq, generating paired-end 150 bp reads. From the.fastq files output by the MiSeq machine, reads were sorted into individual files based on their adapter sequences. Adapter sequences were automatically removed and quality trimming performed by the Illumina software, followed by alignment to the GRCh38 human genome build using Burrows-Wheeler Aligner (BWA) (PMID: 20080505). The Picard software (Broad Institute, Cambridge, MA, USA) was used to remove PCR duplicates and the resulting files were processed using GATK's BaseRecalibrator (Broad Institute) and INDELRealigner tools (Broad Institute) (PMID: 25431634). GATK's haplotypecaller algorithm was used to call mtDNA variants and their heteroplasmy levels were inferred by allelic read depths from the.vcf files.

Transmission electron microscopy

For transmission electron microscopy, cells were fixed at 4 °C overnight, in 2.5% glutaraldehyde/4.0% paraformaldehyde in 0.1 M phosphate buffer and were processed by the electron microscopy facility at Mount Sinai.

Statistical analysis

Disease-specific survival was obtained from patients' medical records and survival analysis was performed using GraphPad Prism software (La Jolla, CA, USA). Reported P-value for survival analysis was calculated using the Log-rank test. Unpaired t-test, Mann–Whitney test or analysis of variance with post-hoc comparisons were used to compare groups, where appropriate. Error bars represent s.e.m.

CONFLICT OF INTEREST

The authors declare no conflict of interest.

AUTHOR CONTRIBUTIONS

TK contributed to the design and interpretation of the data, and has performed the majority of the analysis including western blotting, invasion assays, analysis of mtDNA sequencing data for presentation, preparation of samples for electron microscopy, Seahorse XF Flux Assays and SOD2 scoring statistical analysis. MR has scored the SOD2 slides, established the association with the mitochondria phenotypes and performed the chart review of patients' survival. MS and JC assisted in the Seahorse analysis and the interpretation of the results. AKS and KF have performed the FLIM analysis of tumor sections and guided the interpretation of the results. TL and SG have performed the analysis of the mtDNA sequencing. JS performed the mtDNA repair assay. PH and MB established the stable cell lines overexpressing and inhibiting SOD2 and their characterization, and the analysis of SOD2 staining in metastatic lesions in human samples. AR performed western blot analysis on the cybrids and hybrids. L performed the IHC on SOD2. MDA and GM generated the cybrids and hybrids. DG is the PI and has designed the experiments, interpreted the data and wrote the manuscript.

REFERENCES

1 Viale A, Pettazzoni P, Lyssiotis CA, Ying H, Sanchez N, Marchesini M et al. Oncogene ablation-resistant pancreatic cancer cells depend on mitochondrial function. Nature 2014; **514**: 628–632.

2 Hu J, Hwang SS, Liesa M, Gan B, Sahin E, Jaskelioff M et al. Antitelomerase therapy provokes ALT and mitochondrial adaptive mechanisms in cancer. Cell 2012; **148**: 651–663.

3 LeBleu VS, O'Connell JT, Gonzalez Herrera KN, Wikman H, Pantel K, Haigis MC et al. PGC-1alpha mediates mitochondrial biogenesis and oxidative phosphorylation in cancer cells to promote metastasis. Nat Cell Biol 2014; **16**: 992-1003 1–15.

4 Obre E, Rossignol R. Emerging concepts in bioenergetics and cancer research: metabolic flexibility, coupling, symbiosis, switch, oxidative tumors, metabolic remodeling, signaling and bioenergetic therapy. Int J Biochem Cell Biol 2015; **59**: 167–181.

5 Ishikawa K, Takenaga K, Akimoto M, Koshikawa N, Yamaguchi A, Imanishi H et al. ROS-generating mitochondrial DNA mutations can regulate tumor cell metastasis. Science 2008; **320**: 661–664.

6 Imanishi H, Hattori K, Wada R, Ishikawa K, Fukuda S, Takenaga K et al. Mitochondrial DNA mutations regulate metastasis of human breast cancer cells. PLoS One 2011; **6**: e23401.

7 Hashizume O, Shimizu A, Yokota M, Sugiyama A, Nakada K, Miyoshi H et al. Specific mitochondrial DNA mutation in mice regulates diabetes and lymphoma development. Proc Natl Acad Sci USA 2012; **109**: 10528–10533.

8 Ishikawa K, Imanishi H, Takenaga K, Hayashi J. Regulation of metastasis; mitochondrial DNA mutations have appeared on stage. J Bioenerg Biomembr 2012; **44**: 639–644.

9 Santidrian AF, Matsuno-Yagi A, Ritland M, Seo BB, LeBoeuf SE, Gay LJ et al. Mitochondrial complex I activity and NAD+/NADH balance regulate breast cancer progression. J Clin Invest 2013; **123**: 1068–1081.

10 Yuan Y, Wang W, Li H, Yu Y, Tao J, Huang S et al. Nonsense and missense mutation of mitochondrial ND6 gene promotes cell migration and invasion in human lung adenocarcinoma. BMC Cancer 2015; **15**: 346.

11 Cruz-Bermudez A, Vallejo CG, Vicente-Blanco RJ, Gallardo ME, Fernandez-Moreno MA, Quintanilla M et al. Enhanced tumorigenicity by mitochondrial DNA mild mutations. Oncotarget 2015; **6**: 13628–13643.

12 Nunes JB, Peixoto J, Soares P, Maximo V, Carvalho S, Pinho SS et al. OXPHOS dysfunction regulates integrin-beta1 modifications and enhances cell motility and migration. Hum Mol Genet 2015; **24**: 1977–1990.

13 Jandova J, Janda J, Sligh JE. Changes in mitochondrial DNA alter expression of nuclear encoded genes associated with tumorigenesis. Exp Cell Res 2012; **318**: 2215–2225.

14 Martinus RD, Garth GP, Webster TL, Cartwright P, Naylor DJ, Hoj PB et al. Selective induction of mitochondrial chaperones in response to loss of the mitochondrial genome. Eur J Biochem 1996; **240**: 98–103.

15 Zhao Q, Wang J, Levichkin IV, Stasinopoulos S, Ryan MT, Hoogenraad NJ. A mitochondrial specific stress response in mammalian cells. EMBO J 2002; **21**: 4411–4419.

16 Benedetti C, Haynes CM, Yang Y, Harding HP, Ron D. Ubiquitin-like protein 5 positively regulates chaperone gene expression in the mitochondrial unfolded protein response. Genetics 2006; **174**: 229–239.

17 Fiorese CJ, Schulz AM, Lin YF, Rosin N, Pellegrino MW, Haynes CM. The transcription factor ATF5 mediates a mammalian mitochondrial UPR. Curr Biol 2016; **26**: 2037–2043.

18 Haynes CM, Petrova K, Benedetti C, Yang Y, Ron D. ClpP mediates activation of a mitochondrial unfolded protein response in C. elegans. Dev Cell 2007; **13**: 467–480.

19 Lin YF, Schulz AM, Pellegrino MW, Lu Y, Shaham S, Haynes CM. Maintenance and propagation of a deleterious mitochondrial genome by the mitochondrial unfolded protein response. Nature 2016; **533**: 416–419.

20 Mohrin M, Shin J, Liu Y, Brown K, Luo H, Xi Y et al. Stem cell aging. A mitochondrial UPR-mediated metabolic checkpoint regulates hematopoietic stem cell aging. Science 2015; **347**: 1374–1377.

21 Nargund AM, Fiorese CJ, Pellegrino MW, Deng P, Haynes CM. Mitochondrial and nuclear accumulation of the transcription factor ATFS-1 promotes OXPHOS recovery during the UPR(mt). Mol Cell 2015; **58**: 123–133.

22 Nargund AM, Pellegrino MW, Fiorese CJ, Baker BM, Haynes CM. Mitochondrial import efficiency of ATFS-1 regulates mitochondrial UPR activation. Science 2012; **337**: 587–590.

23 Durieux J, Wolff S, Dillin A. The cell-non-autonomous nature of electron transport chain-mediated longevity. Cell 2011; **144**: 79–91.

24 Tian Y, Merkwirth C, Dillin A, Mitochondrial UPR, Double-Edged Sword. A. Trends Cell Biol 2016; **26**: 563–565.

25 Munch C, Harper JW. Mitochondrial unfolded protein response controls matrix pre-RNA processing and translation. Nature 2016; **534**: 710–713.

26 Papa L, Germain D. Estrogen receptor mediates a distinct mitochondrial unfolded protein response. *J Cell Sci* 2011; **124**(Pt 9): 1396–1402.

27 Papa L, Germain D. SirT3 regulates the mitochondrial unfolded protein response. *Mol Cell Biol* 2014; **34**: 699–710.

28 Palacios OM, Carmona JJ, Michan S, Chen KY, Manabe Y, Ward JL 3rd *et al*. Diet and exercise signals regulate SIRT3 and activate AMPK and PGC-1alpha in skeletal muscle. *Aging* 2009; **1**: 771–783.

29 Pillai VB, Sundaresan NR, Kim G, Gupta M, Rajamohan SB, Pillai JB *et al*. Exogenous NAD blocks cardiac hypertrophic response via activation of the SIRT3-LKB1-AMP-activated kinase pathway. *J Biol Chem* 2010; **285**: 3133–3144.

30 Shi T, Fan GQ, Xiao SD. SIRT3 reduces lipid accumulation via AMPK activation in human hepatic cells. *J Dig Dis* 2010; **11**: 55–62.

31 Mouchiroud L, Houtkooper RH, Moullan N, Katsyuba E, Ryu D, Canto C *et al*. The NAD(+)/Sirtuin pathway modulates longevity through activation of mitochondrial UPR and FOXO signaling. *Cell* 2013; **154**: 430–441.

32 Houtkooper RH, Pirinen E, Auwerx J. Sirtuins as regulators of metabolism and healthspan. *Nat Rev Mol Cell Biol* 2012; **13**: 225–238.

33 Lombard DB, Tishkoff DX, Bao J. Mitochondrial sirtuins in the regulation of mitochondrial activity and metabolic adaptation. *Handb Exp Pharmacol* 2011; **206**: 163–188.

34 Riggins RB, Zwart A, Nehra R, Clarke R. The nuclear factor kappa B inhibitor parthenolide restores ICI 182,780 (Faslodex; fulvestrant)-induced apoptosis in antiestrogen-resistant breast cancer cells. *Mol Cancer Ther* 2005; **4**: 33–41.

35 Andrews RM, Kubacka I, Chinnery PF, Lightowlers RN, Turnbull DM, Howell N. Reanalysis and revision of the Cambridge reference sequence for human mitochondrial DNA. *Nat Genet* 1999; **23**: 147.

36 Yuzefovych LV, Kahn AG, Schuler MA, Eide L, Arora R, Wilson GL *et al*. Mitochondrial DNA repair through OGG1 activity attenuates breast cancer progression and metastasis. *Cancer Res* 2016; **76**: 30–34.

37 Hart PC, Mao M, de Abreu AL, Ansenberger-Fricano K, Ekoue DN, Ganini D *et al*. MnSOD upregulation sustains the Warburg effect via mitochondrial ROS and AMPK-dependent signalling in cancer. *Nat Commun* 2015; **6**: 6053.

38 Desmetz C, Bibeau F, Boissiere F, Bellet V, Rouanet P, Maudelonde T *et al*. Proteomics-based identification of HSP60 as a tumor-associated antigen in early stage breast cancer and ductal carcinoma in situ. *J Proteome Res* 2008; **7**: 3830–3837.

39 Rappa F, Pitruzzella A, Marino Gammazza A, Barone R, Mocciaro E, Tomasello G *et al*. Quantitative patterns of Hsps in tubular adenoma compared with normal and tumor tissues reveal the value of Hsp10 and Hsp60 in early diagnosis of large bowel cancer. *Cell Stress Chaperones* 2016; **21**: 927–933.

40 D'Aurelio M, Gajewski CD, Lin MT, Mauck WM, Shao LZ, Lenaz G *et al*. Heterologous mitochondrial DNA recombination in human cells. *Hum Mol Genet* 2004; **13**: 3171–3179.

41 Ragazzi M, de Biase D, Betts CM, Farnedi A, Ramadan SS, Tallini G *et al*. Oncocytic carcinoma of the breast: frequency, morphology and follow-up. *Hum Pathol* 2011; **42**: 166–175.

42 Tao R, Coleman MC, Pennington JD, Ozden O, Park SH, Jiang H *et al*. Sirt3-mediated deacetylation of evolutionarily conserved lysine 122 regulates MnSOD activity in response to stress. *Mol Cell* 2010; **40**: 893–904.

43 Conklin MW, Provenzano PP, Eliceiri KW, Sullivan R, Keely PJ. Fluorescence lifetime imaging of endogenous fluorophores in histopathology sections reveals differences between normal and tumor epithelium in carcinoma *in situ* of the breast. *Cell Biochem Biophys* 2009; **53**: 145–157.

44 Feeley KP, Bray AW, Westbrook DG, Johnson LW, Kesterson RA, Ballinger SW *et al*. Mitochondrial genetics regulate breast cancer tumorigenicity and metastatic potential. *Cancer Res* 2015; **75**: 4429–4436.

45 Takibuchi G, Imanishi H, Morimoto M, Ishikawa K, Nakada K, Toyama-Sorimachi N *et al*. Polymorphic mutations in mouse mitochondrial DNA regulate a tumor phenotype. *Mitochondrion* 2013; **13**: 881–887.

46 McMahon S, LaFramboise T. Mutational patterns in the breast cancer mitochondrial genome, with clinical correlates. *Carcinogenesis* 2014; **35**: 1046–1054.

47 Bai RK, Leal SM, Covarrubias D, Liu A, Wong LJ. Mitochondrial genetic background modifies breast cancer risk. *Cancer Res* 2007; **67**: 4687–4694.

48 Covarrubias D, Bai RK, Wong LJ, Leal SM. Mitochondrial DNA variant interactions modify breast cancer risk. *J Hum Genet.* 2008; **53**: 924–928.

49 van Waveren C, Sun Y, Cheung HS, Moraes CT. Oxidative phosphorylation dysfunction modulates expression of extracellular matrix--remodeling genes and invasion. *Carcinogenesis* 2006; **27**: 409–418.

50 Finley LW, Carracedo A, Lee J, Souza A, Egia A, Zhang J *et al*. SIRT3 opposes reprogramming of cancer cell metabolism through HIF1alpha destabilization. *Cancer Cell* 2011; **19**: 416–428.

51 Papa L, Hahn M, Marsh EL, Evans BS, Germain D. SOD2 to SOD1 switch in breast cancer. *J Biol Chem* 2014; **289**: 5412–5416.

52 Yang W, Nagasawa K, Munch C, Xu Y, Satterstrom K, Jeong S *et al*. Mitochondrial sirtuin network reveals dynamic SIRT3-dependent deacetylation in response to membrane depolarization. *Cell* 2016; **167**: 985–1000 e21.

53 Seo JH, Rivadeneira DB, Caino MC, Chae YC, Speicher DW, Tang HY *et al*. The mitochondrial unfoldase-peptidase complex ClpXP controls bioenergetics stress and metastasis. *PLoS Biol* 2016; **14**: e1002507.

54 Serasinghe MN, Wieder SY, Renault TT, Elkholi R, Asciolla JJ, Yao JL *et al*. Mitochondrial division is requisite to RAS-induced transformation and targeted by oncogenic MAPK pathway inhibitors. *Mol Cell* 2015; **57**: 521–536.

Supplementary Information accompanies this paper on the Oncogene website (http://www.nature.com/onc)